minerals

MDPI

Supplementary materials

The Viscosity and Atomic Structure of Volatile-Bearing Melilititic Melts at High Pressure and Temperature and the Transport of Deep Carbon

Vincenzo Stagno [1,2,*], Veronica Stopponi [1], Yoshio Kono [3], Annalisa D'Arco [4], Stefano Lupi [4,5], Claudia Romano [6], Brent T. Poe [7], Dionysis I. Foustoukos [8], Piergiorgio Scarlato [2] and Craig E. Manning [9]

1 Department of Earth Sciences, Sapienza University of Rome, 00185 Rome, Italy; veronica.stopponi@uniroma1.it
2 National Institute of Geophysics and Volcanology, 00143 Rome, Italy; piergiorgio.scarlato@ingv.it
3 Geodynamics Research Center, Ehime University, 790-8577 Matsuyama, Japan; kono.yoshio.rj@ehime-u.ac.jp
4 INFN National Institute of Nuclear Physics, 00185 Rome, Italy; annalisa.darco@roma1.infn.it (A.D.); stefano.lupi@roma1.infn.it (S.L.)
5 CNR-IOM and Department of Physics, Sapienza University of Rome, 00185 Rome, Italy
6 Department of Sciences, University of Studies Roma Tre, L.go San Leonardo Murialdo 1, 00146 Rome, Italy; claudia.romano@uniroma3.it
7 Department of Engineering and Geology, University of Chieti-Pescara, 66013 Chieti Scalo, Italy; brent.poe@unich.it
8 Geophysical Laboratory, Carnegie Institution of Washington, Washington, DC 20015, USA; dfoustoukos@ciw.edu
9 Department of Earth, Planetary and Space Sciences, University of California, Los Angeles, CA 90095, USA; manning@epss.ucla.edu
* Correspondence: vincenzo.stagno@uniroma1.it

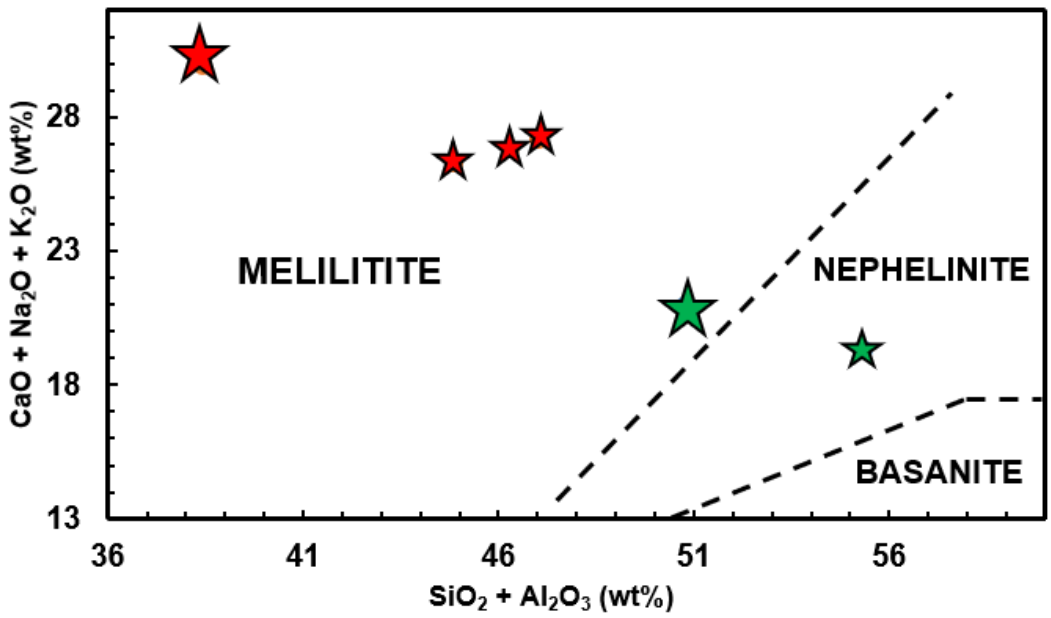

Figure S1. Diagram proposed by Le Bas (1989) for the classification of foiditic rocks. Big stars are representative of FOID1 (green) and FOID2 (red) starting materials. Small stars are the compositions of the recovered glasses from experiments listed in Table 3 of the main text.

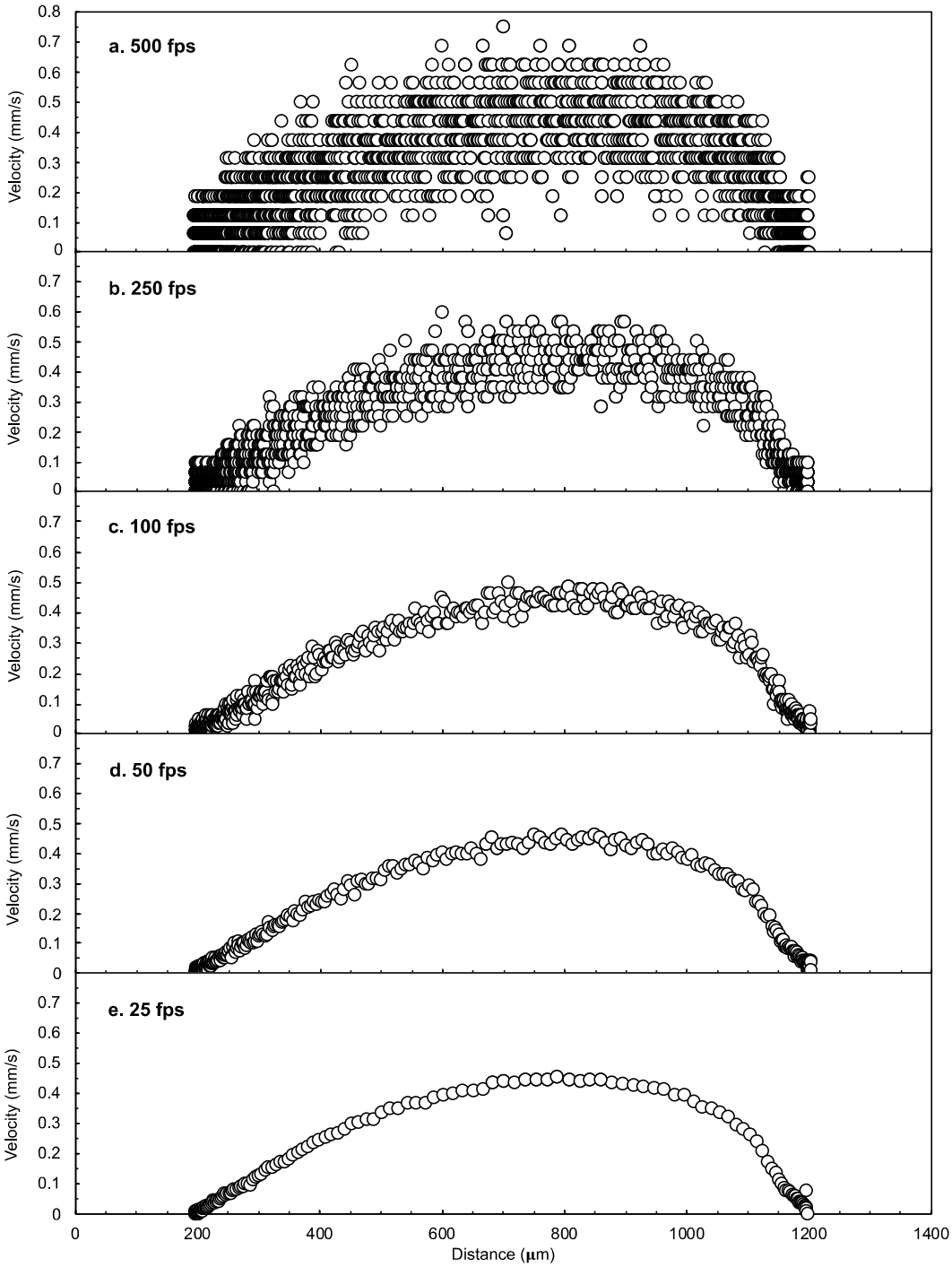

Figure S2. A simulation of falling velocity analysis with varying camera frame rate for the FOID1_run2 at 4.7 GPa and 1755 °C.

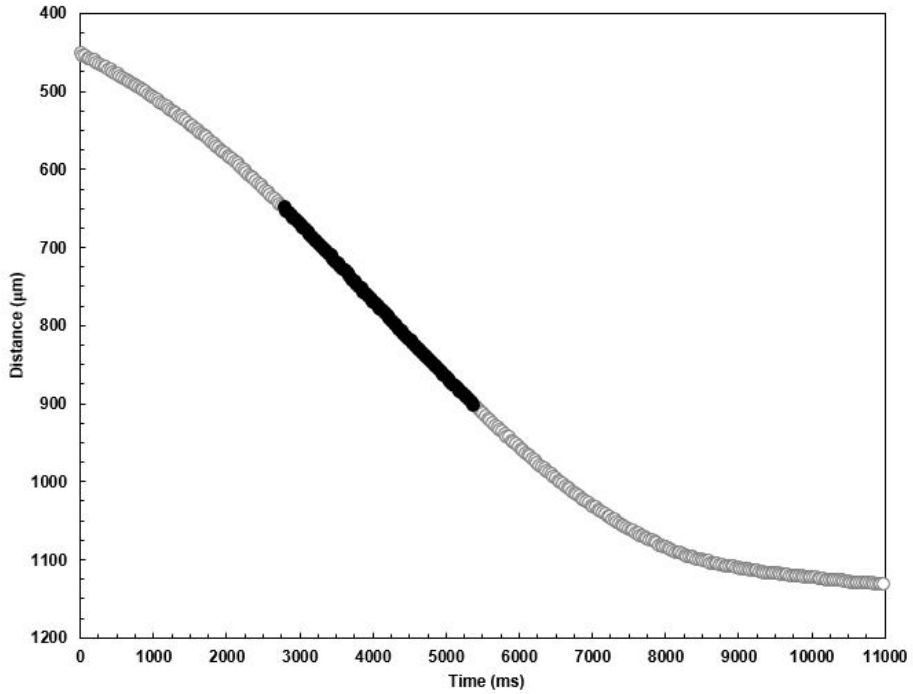

Figure S3. Results of the falling distance of the Pt sphere (120 μm) for the run at 2.5 GPa and 1580 °C (FOID1_RUN1) as function of time.

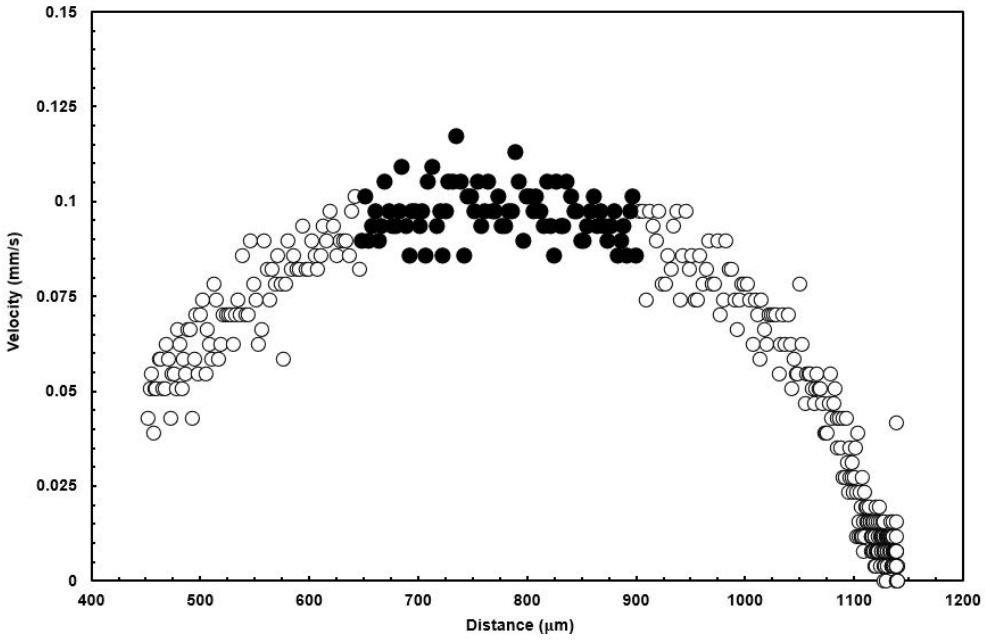

Figure S4. Results of the falling velocity of the Pt sphere for the run at 2.5 GPa and 1580 °C (FOID1_RUN1).

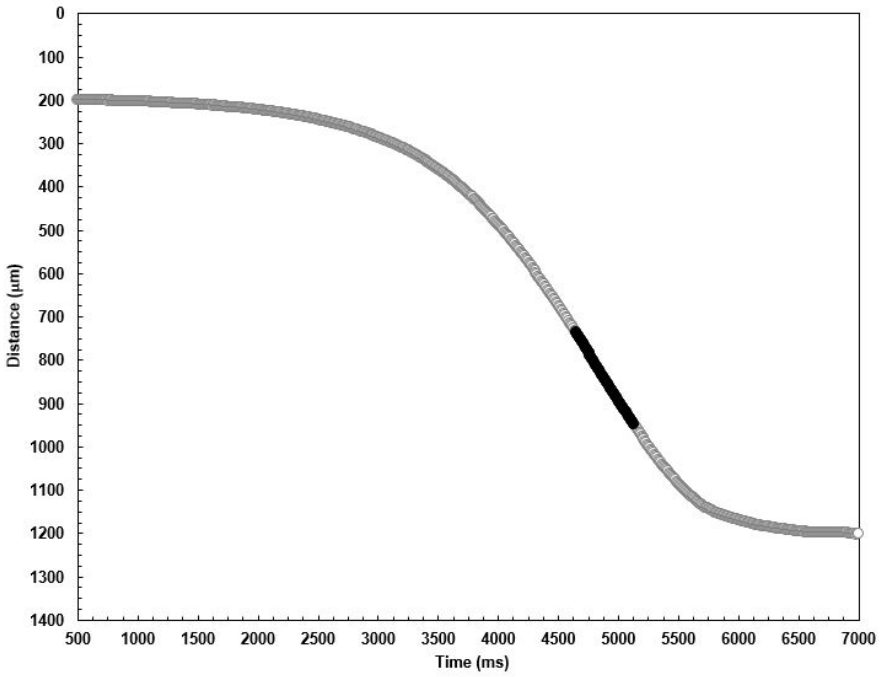

Figure S5. Results of the falling distance of the Pt sphere (121 μm) for the run at 4.7 GPa and 1755 °C as function of time.

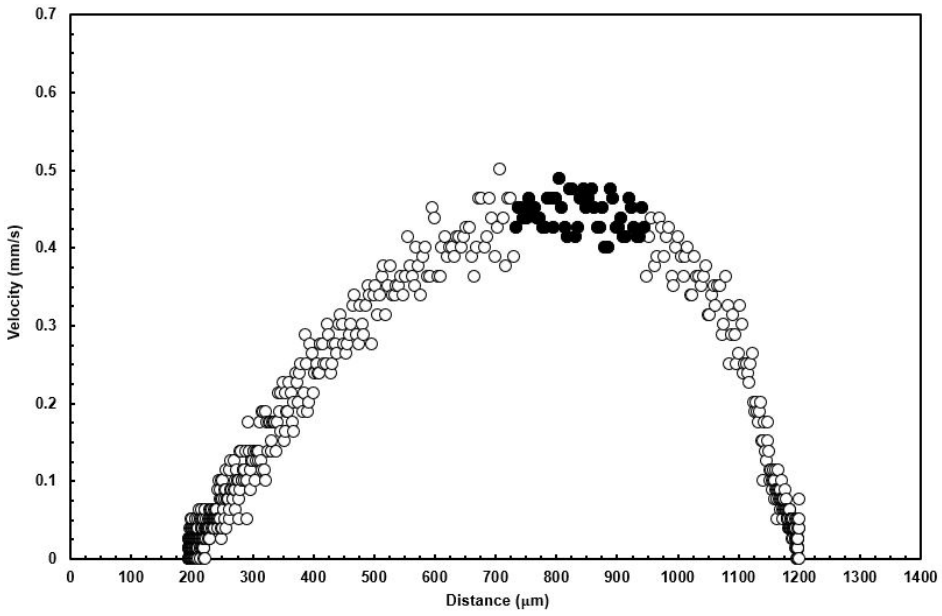

Figure S6. Results of the falling velocity of the Pt sphere for the run at 4.7 GPa and 1755 °C (FOID1_RUN2).

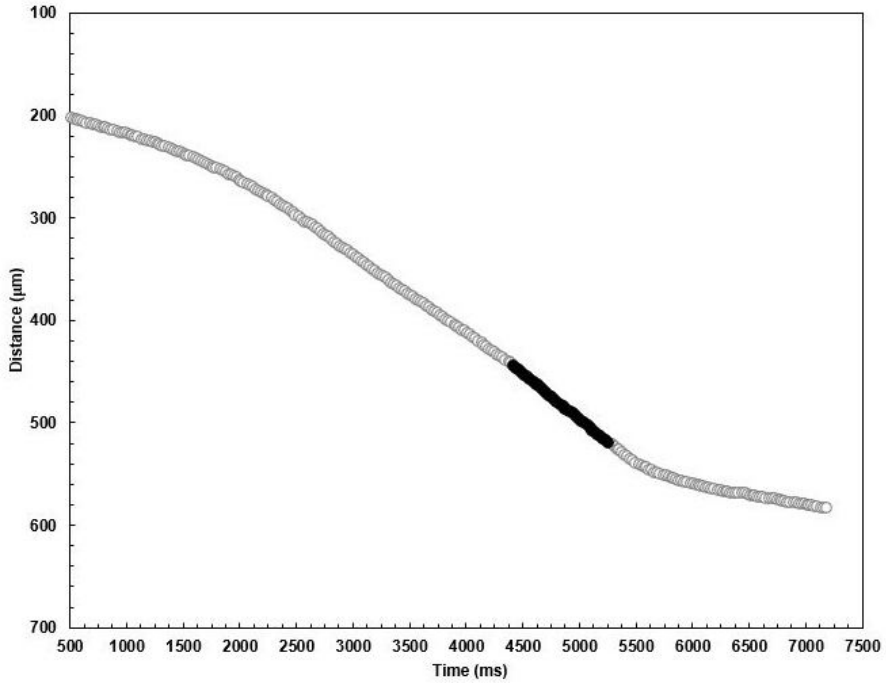

Figure S7. Results of the falling distance of the Pt sphere (85 μm) for the run at 4.2 GPa and 1700 °C (FOID1_RUN3) as function of time.

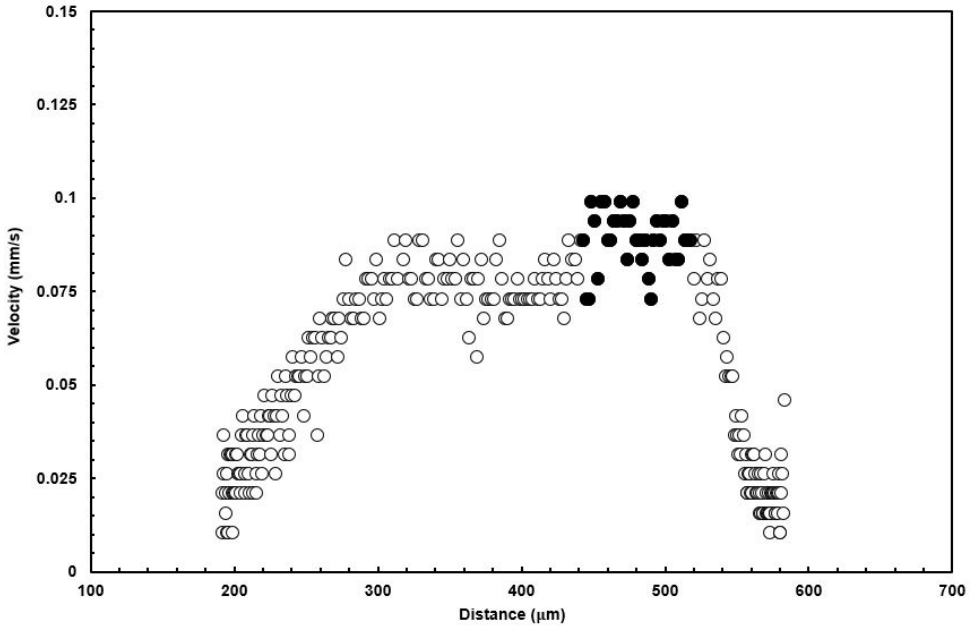

Figure S8. Results of the falling velocity of the Pt sphere for the run at 4.2 GPa and 1700 °C (FOID1_RUN3).

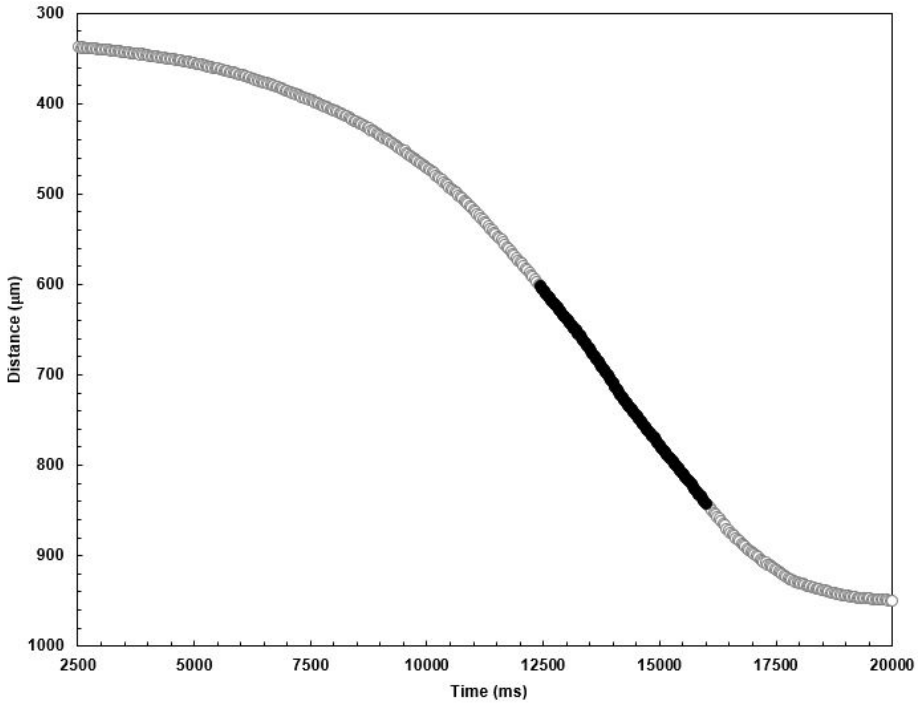

Figure S9. Results of the falling distance of the Pt sphere (146 μm) for the run at 1 GPa and 1270 °C (FOID2_RUN1) as function of time.

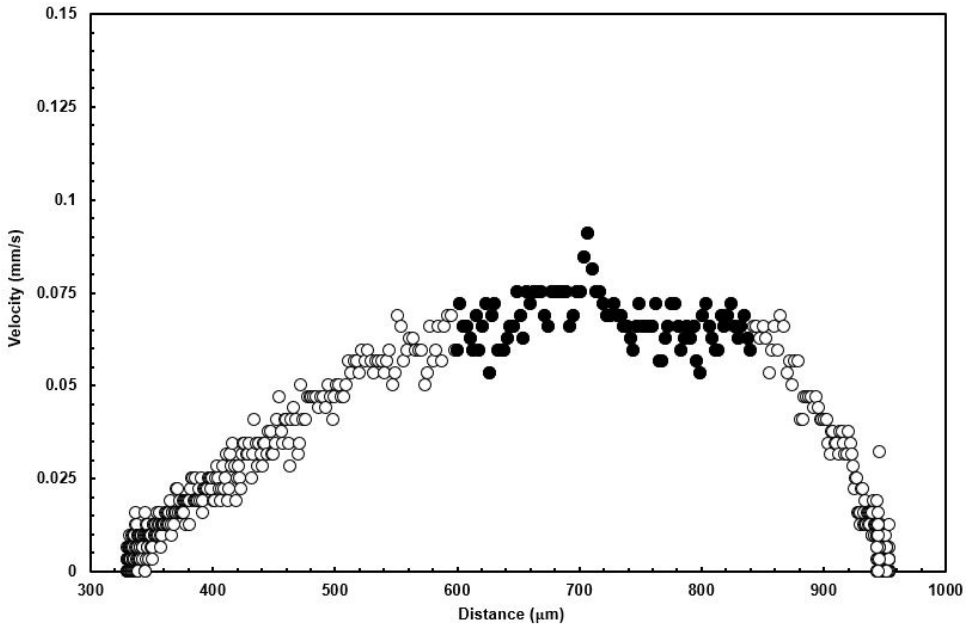

Figure S10. Results of the falling velocity of the Pt sphere for the run at 1 GPa and 1270 °C (FOID2_RUN1).

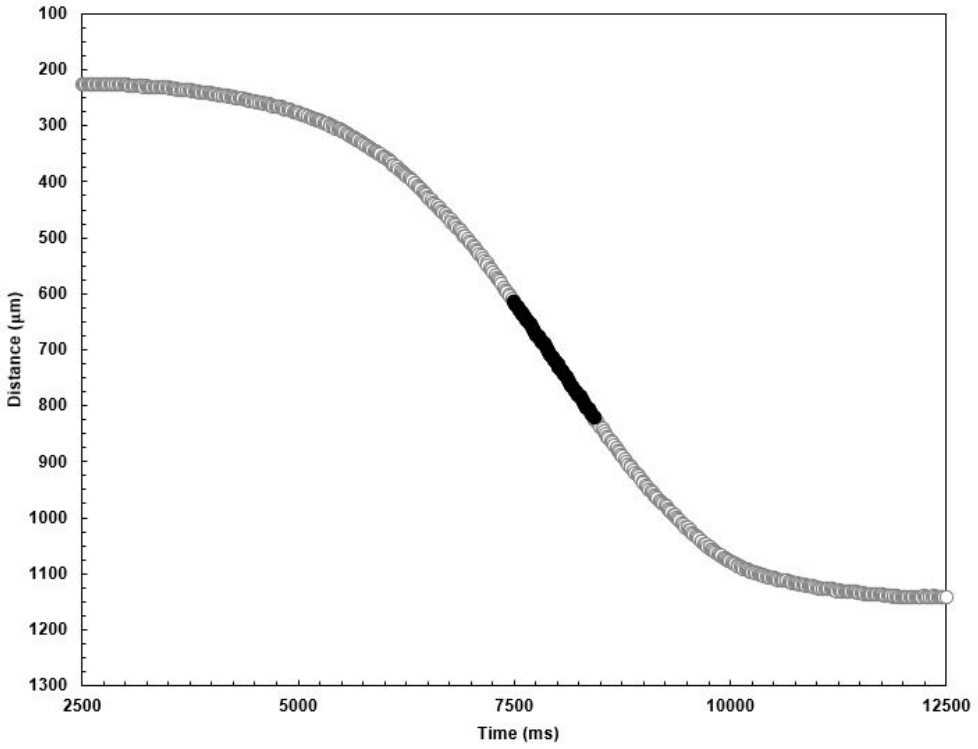

Figure S11. Results of the falling distance of the Pt sphere (142 μm) for the run at 3.4 GPa and 1360 °C (FOID2_RUN2) as function of time.

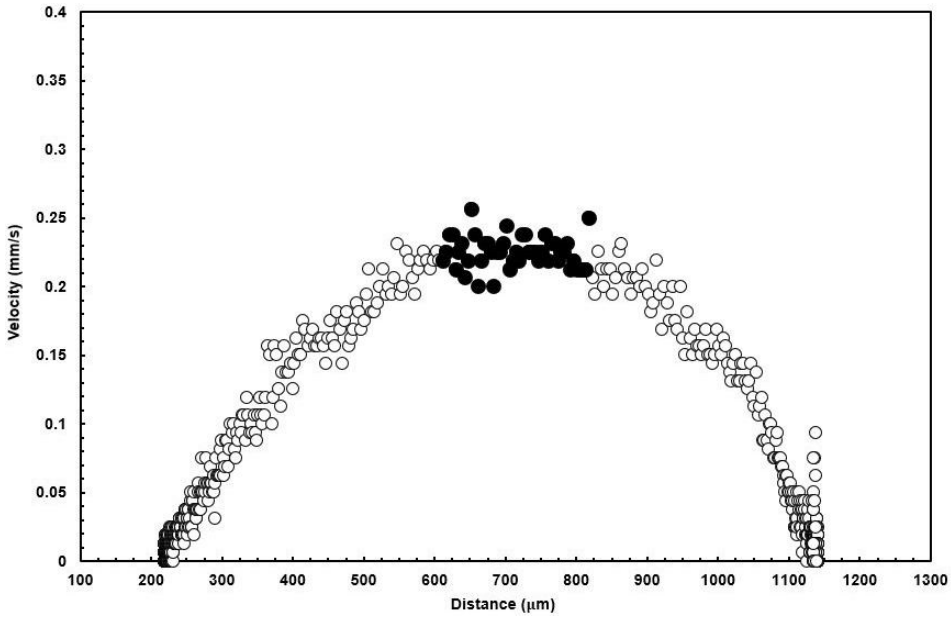

Figure S12. Results of the falling velocity of the Pt sphere for the run at 3.4 GPa and 1360 °C (FOID2_RUN2).

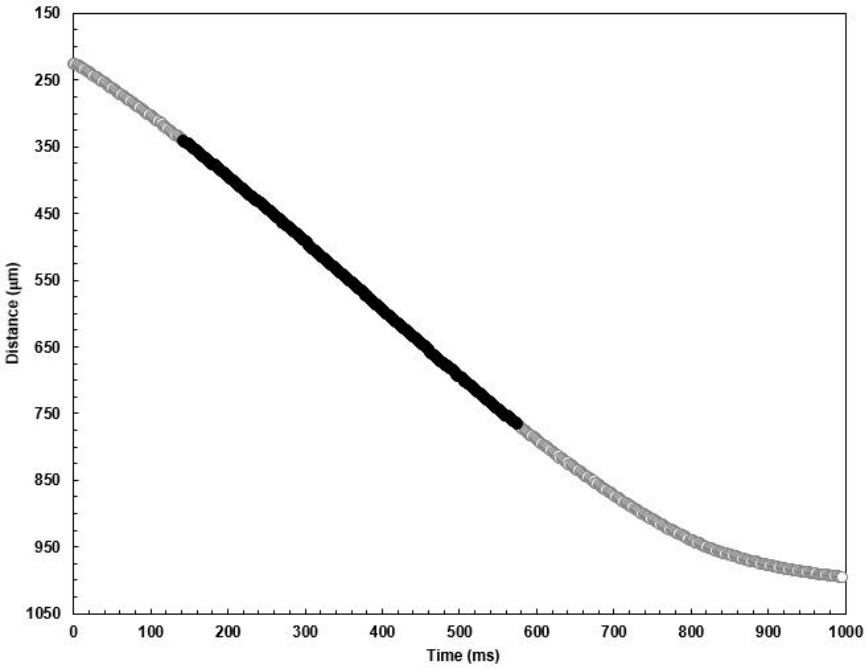

Figure S13. Results of the falling distance of the Pt sphere (104 μm) for the run at 4.5 GPa and 1540 °C (FOID2_RUN3) as function of time.

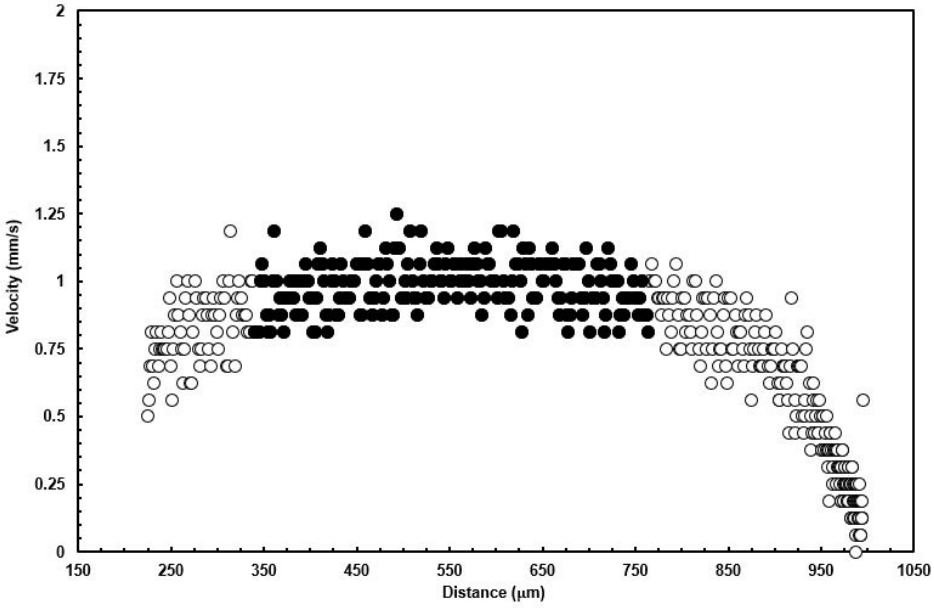

Figure S14. Results of the falling velocity of the Pt sphere for the run at 4.5 GPa and 1540 °C (FOID2_RUN3).

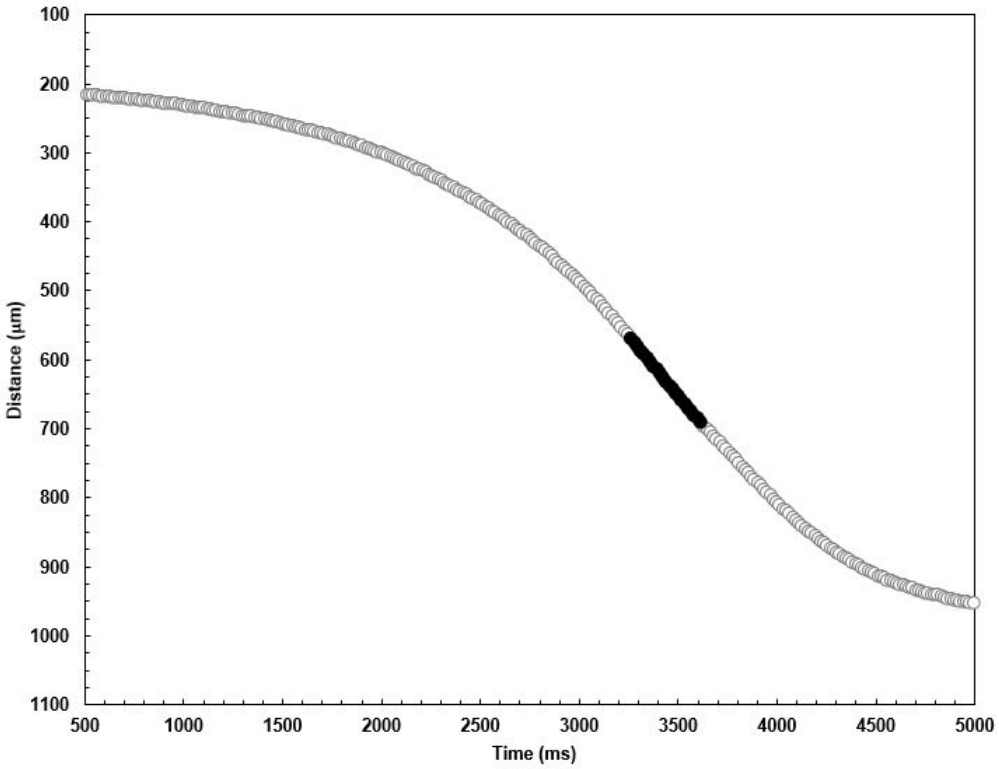

Figure S15. Results of the falling distance of the Pt sphere (134 μm) placed at the capsule edge for the run at 1.7 GPa and 1265 °C (FOID2_2018) as function of time.

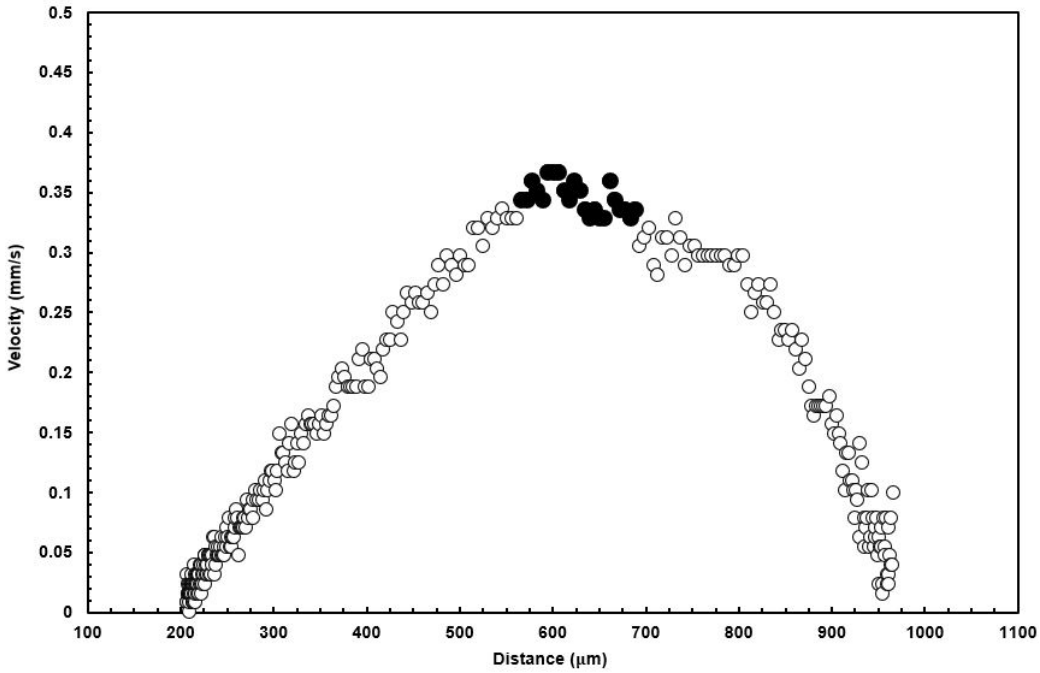

Figure S16. Results of the falling velocity of the Pt sphere for the run at 1.7 GPa and 1265 °C (FOID2_2018_edge).

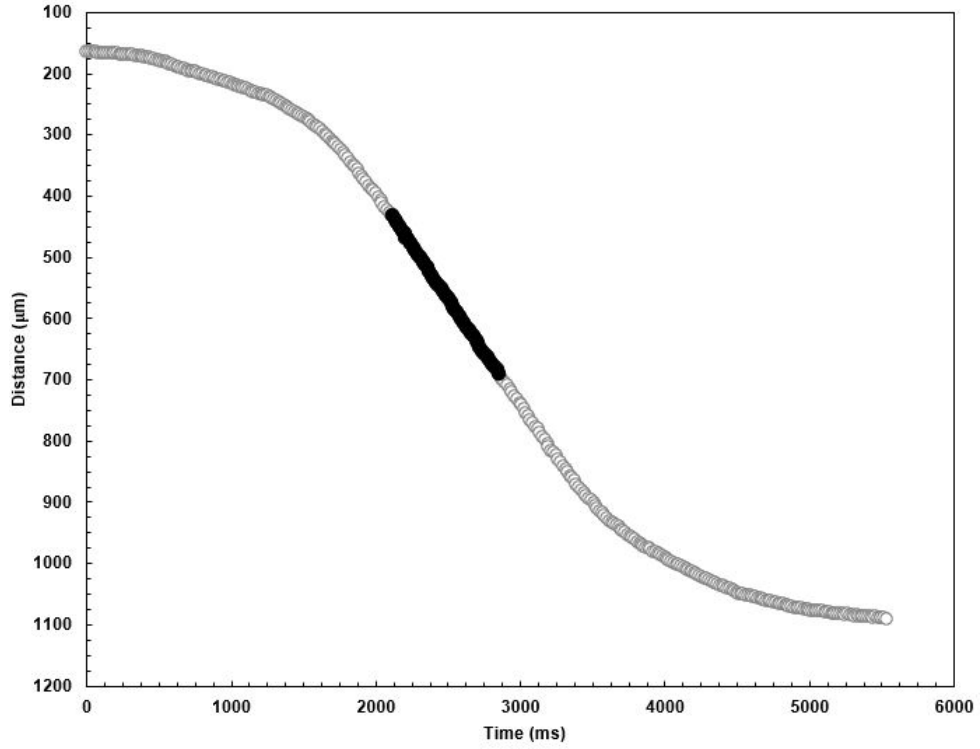

Figure S17. Results of the falling distance of the Pt sphere (131 μm) for the run at 1.7 GPa and 1265 °C (FOID2_2018_center) as function of time.

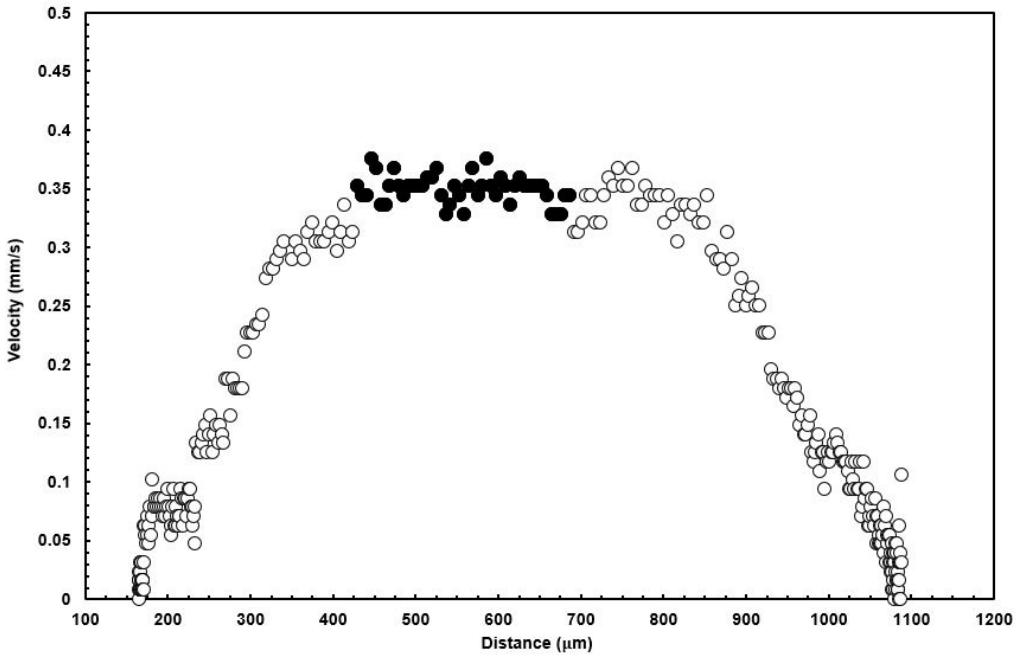

Figure S18. Results of the falling velocity of the Pt sphere for the run at 1.7 GPa and 1265 °C (FOID2_2018_center).

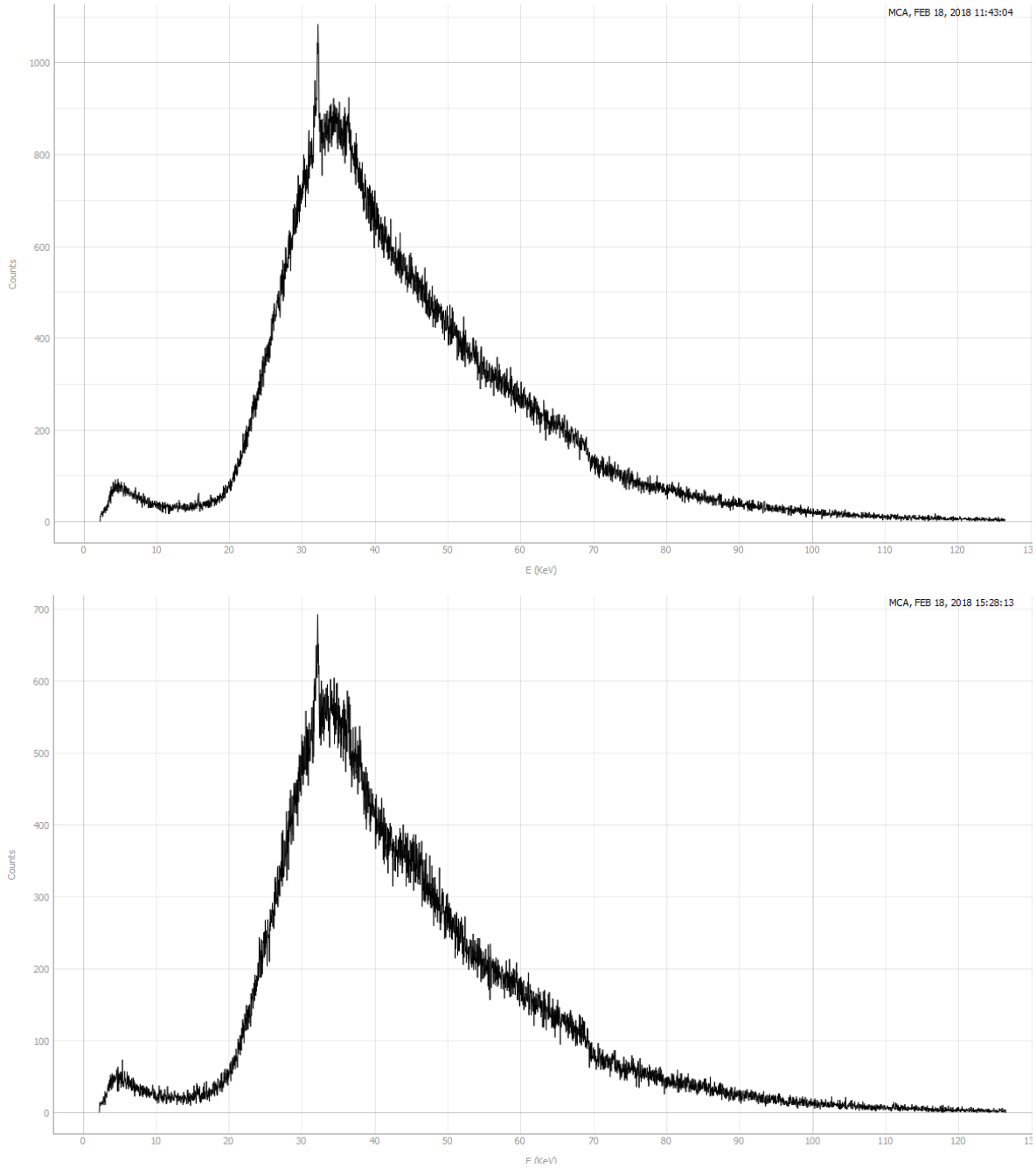

Figure S19. EDXD pattern of FOID1_RUN3_2018 a) before and b) after quenching from melt structure measurements.

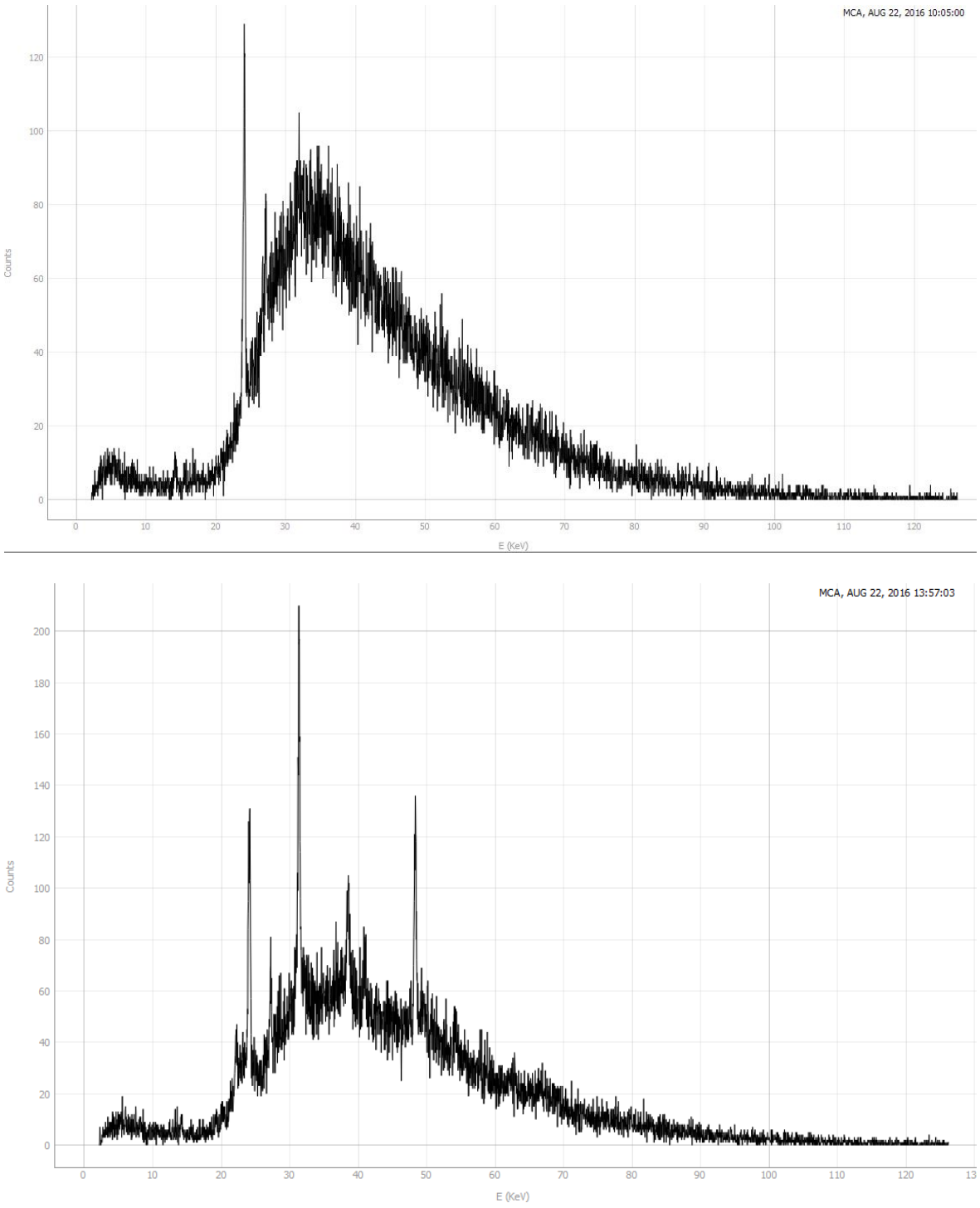

Figure S20. EDXD pattern of FOID2_RUN2 a) before and b) after melt structure measurements.

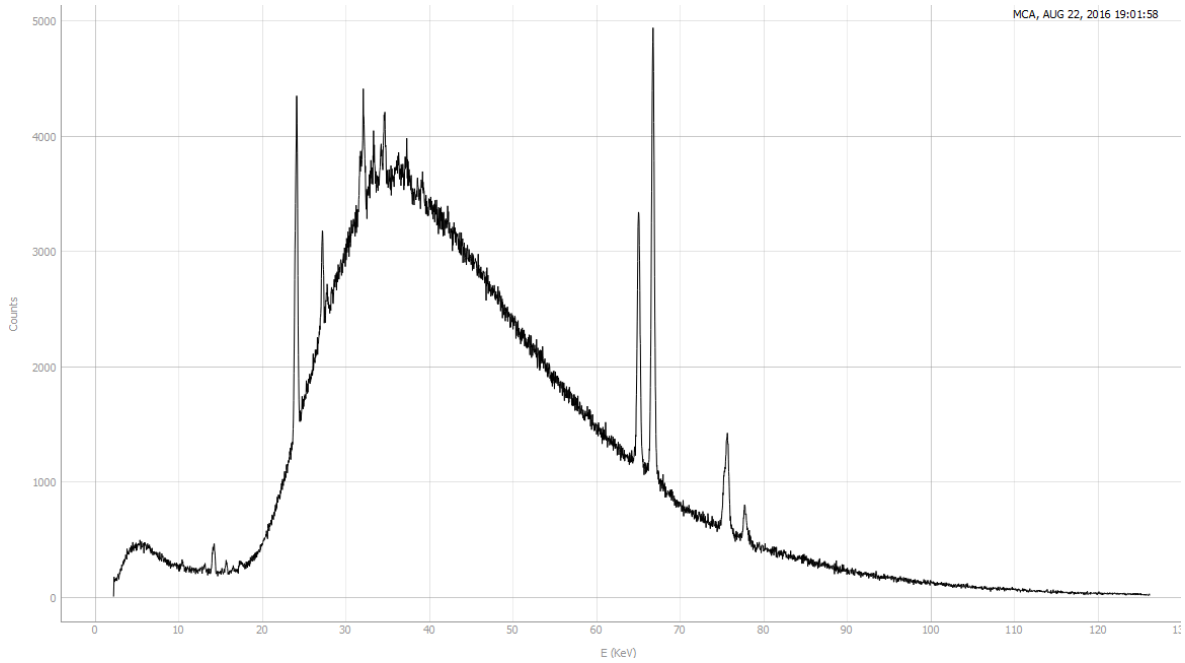

Figure S21. EDXD pattern of FOID2_RUN3 just before melt structure measurements ended at 2θ of 28°.

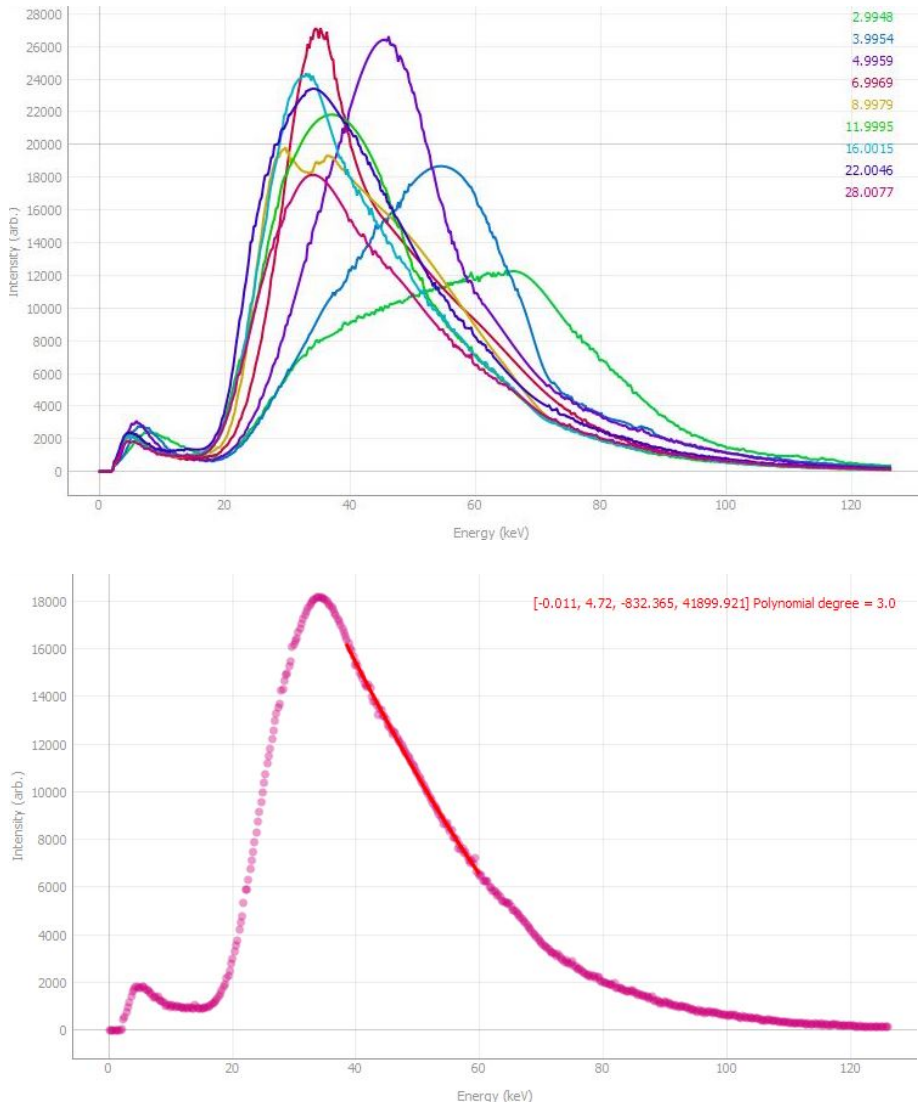

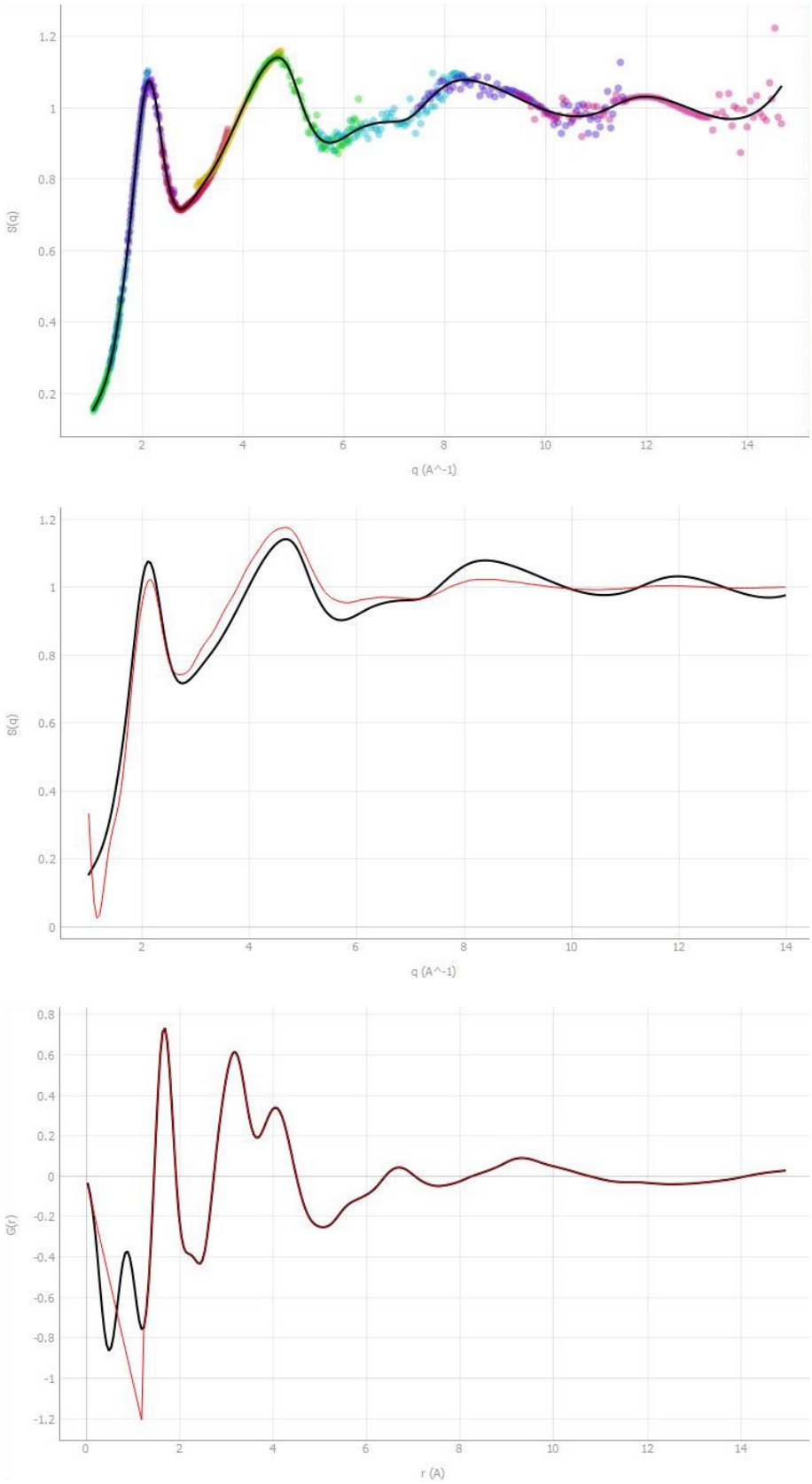

Figure S22. (a) Multi-angle energy dispersive X-ray diffraction spectra from FOID1_RUN3_2018; (b) the effective primary beam estimation for a selected energy range; (c) total structure factor S(q) composed of the fragmented structure factor scaled with respect to the highest angle fragment. The solid line is obtained after error-weighted spline-smoothening of the overlapped structure factor fragments.

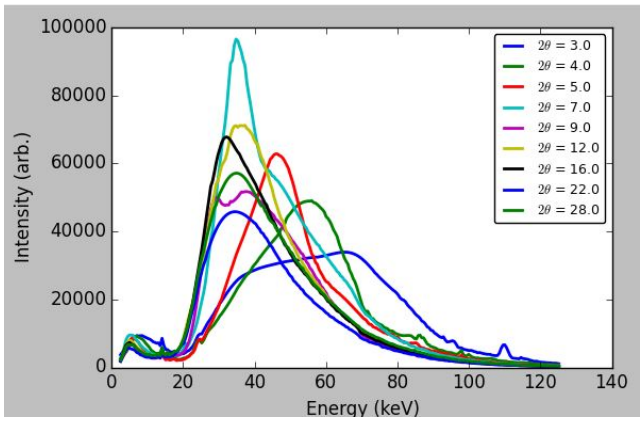
Intensity (arb.)
Energy (keV)
2θ = 3.0
2θ = 4.0
2θ = 5.0
2θ = 7.0
2θ = 9.0
2θ = 12.0
2θ = 16.0
2θ = 22.0
2θ = 28.0

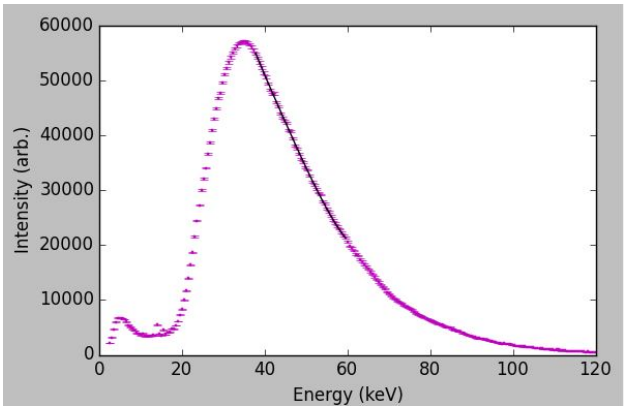
Intensity (arb.)
Energy (keV)

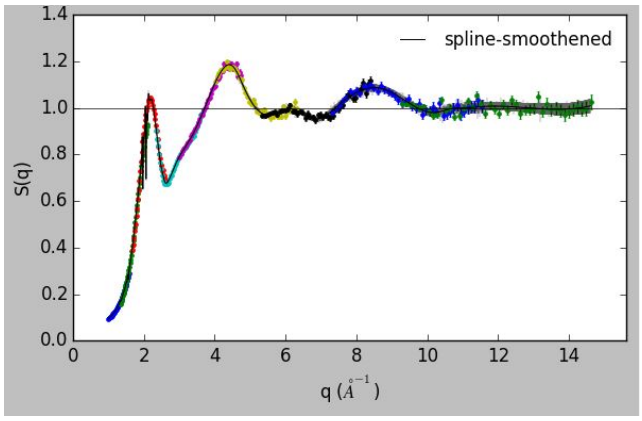
spline-smoothened
S(q)
q ($\AA^{-1}$)

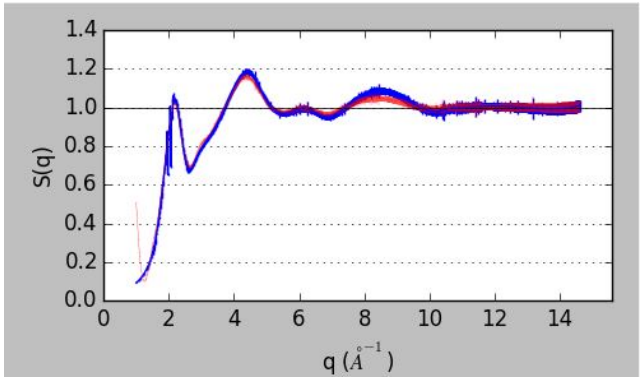
S(q)
q ($\AA^{-1}$)

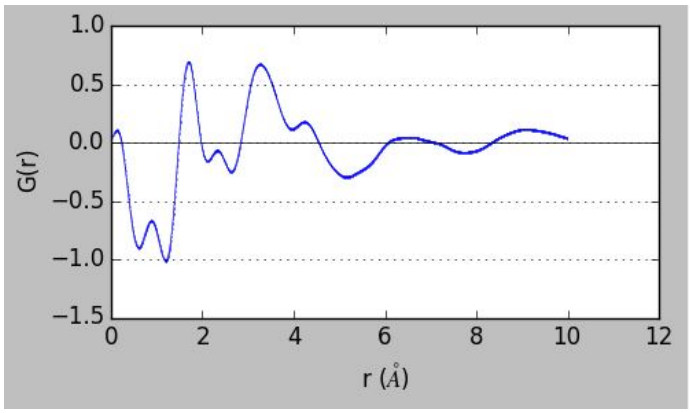

Figure S23. (a) Multi-angle energy dispersive X-ray diffraction spectra from FOID2_RUN2; (b) the effective primary beam estimation for a selected energy range; (c) total structure factor S(q) composed of the fragmented structure factor scaled with respect to the highest angle fragment. The solid line is obtained after error-weighted spline-smoothening of the overlapped structure factor fragments; d) Structure factor S(q) and (e) reduced pair distribution function G(r).

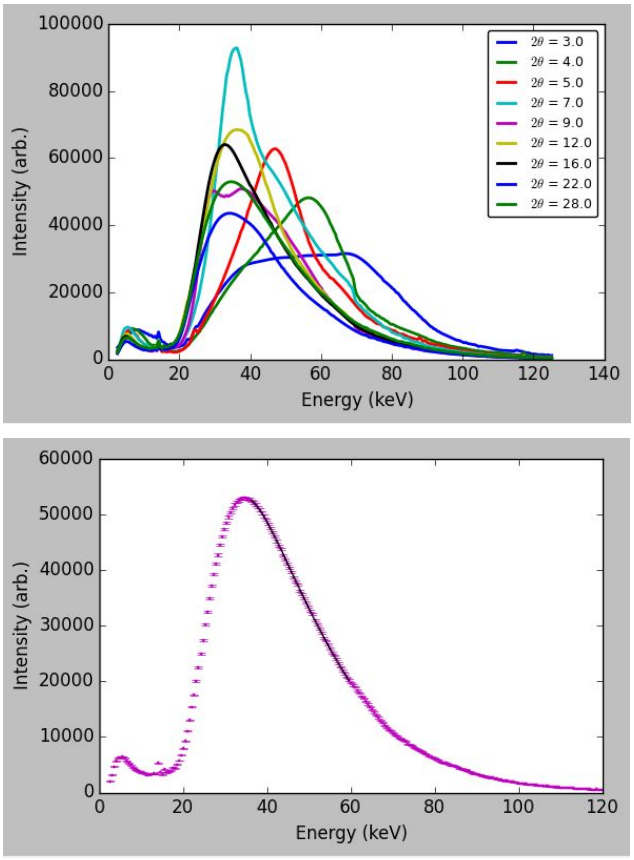

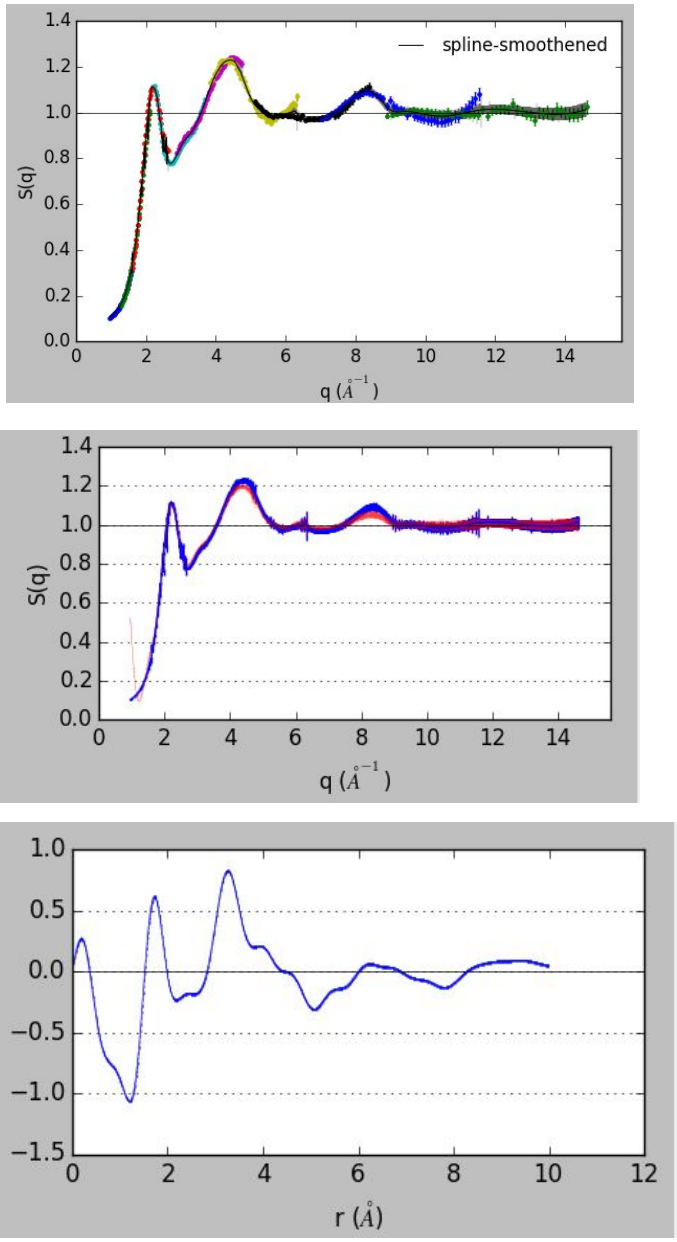

Figure S24. (a) Multi-angle energy dispersive X-ray diffraction spectra from FOID2_RUN3; (b) the effective primary beam estimation for a selected energy range; (c) total structure factor S(q) composed of the fragmented structure factor scaled with respect to the highest angle fragment. The solid line is obtained after error-weighted spline-smoothening of the overlapped structure factor fragments; d) Structure factor S(q) and (e) reduced pair distribution function G(r).

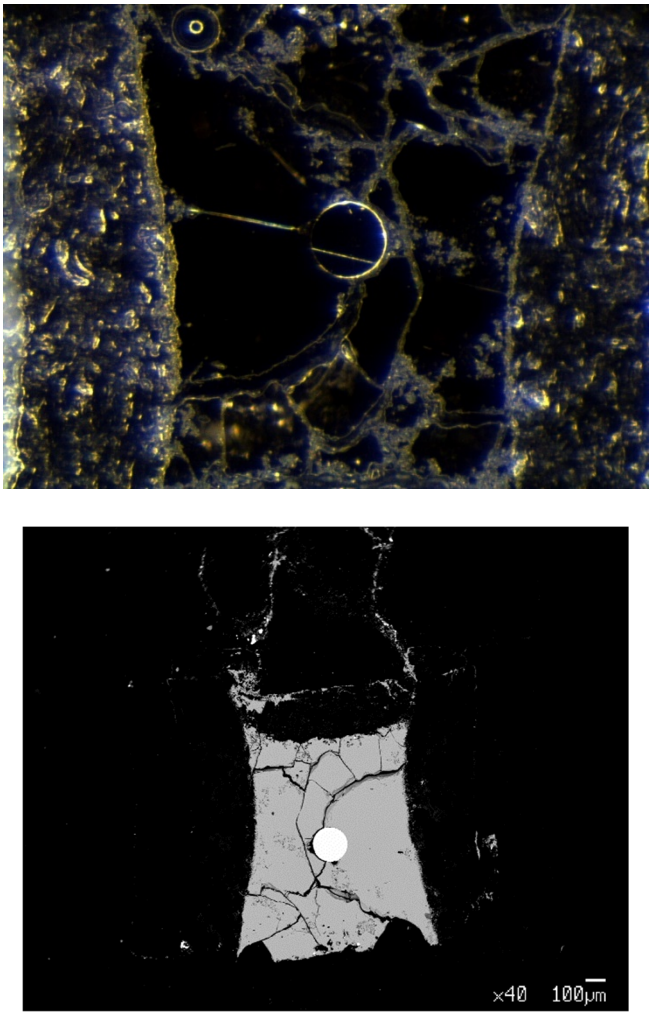

Figure S25. Images of the polished FOID1_RUN3_2018 run product collected under optical microscope (left panel) and back-scattered electron (right panel).

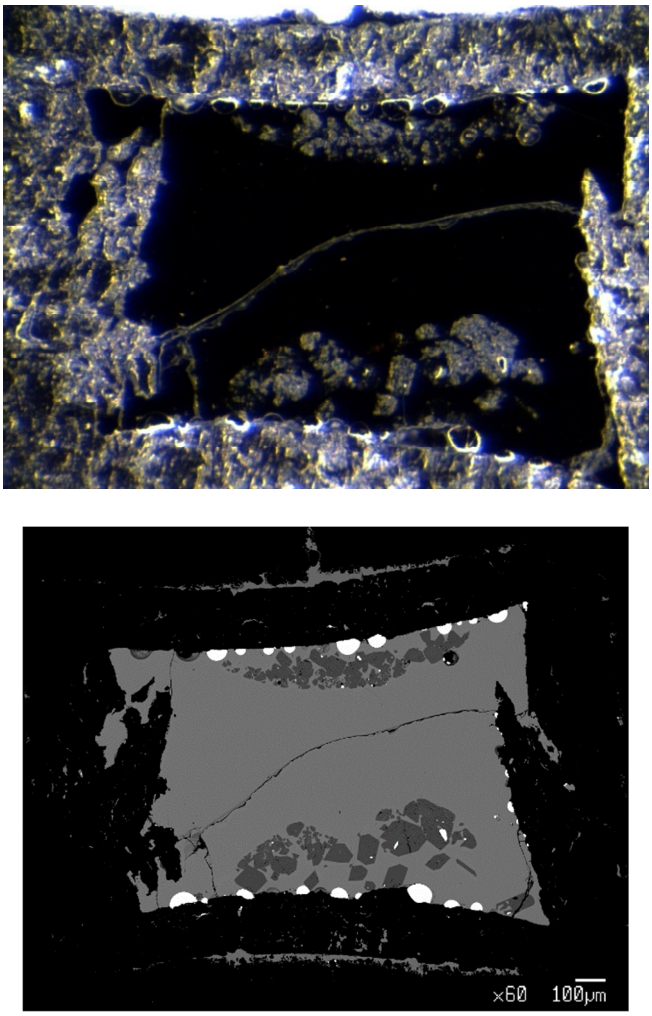

Figure S26. Images of the polished FOID2_RUN1 run product collected under optical microscope (left panel) and back-scattered electron (right panel).

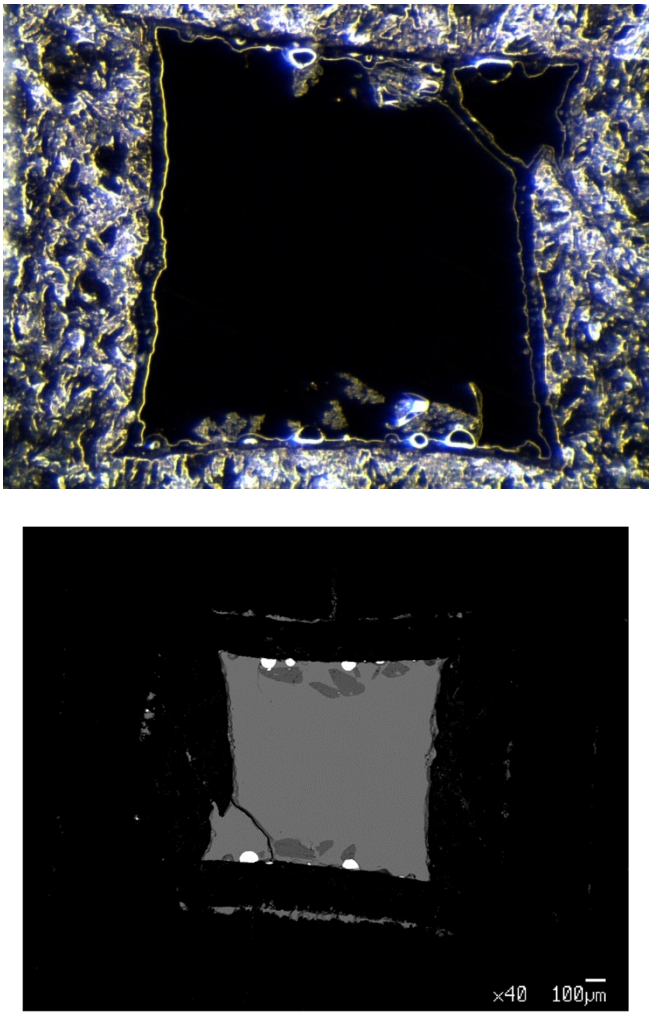

Figure S27. Images of the polished FOID2_RUN2 run product collected under optical microscope (left panel) and back-scattered electron (right panel).

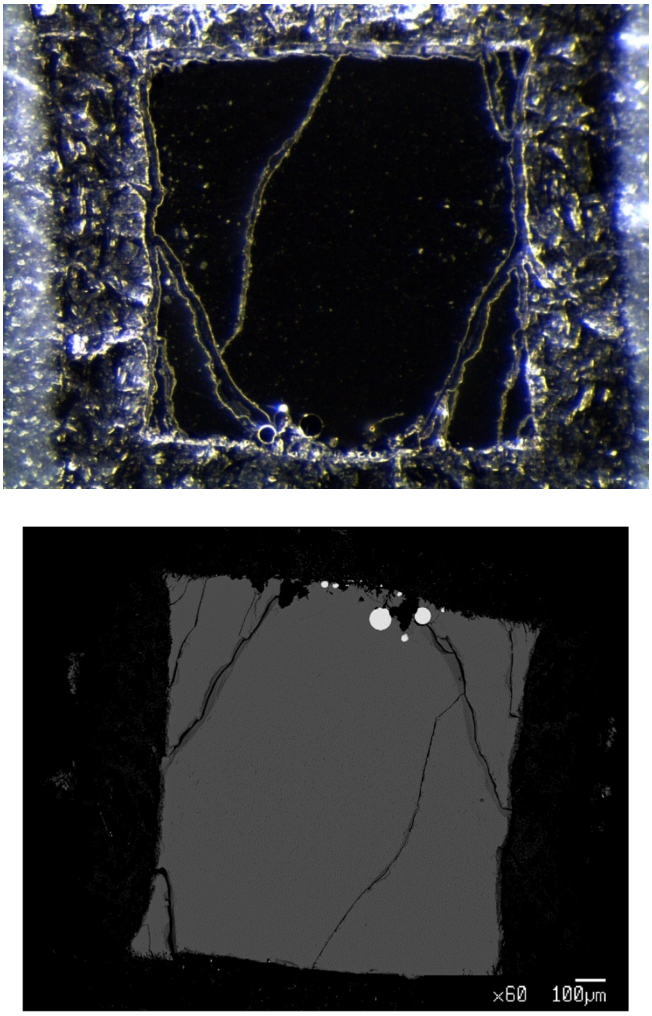

Figure S28. Images of the polished FOID2_RUN3 run product collected under optical microscope (left panel) and back-scattered electron (right panel).

Table S1. EMPA results of recovered quenched glasses after melt structure measurements.

	FOID1_RUN3_2018	*FOID2_RUN1*	*FOID2_RUN2*	*FOID2_RUN3*
No. of points analyzed	**9**	*8*	*8*	*8*
P/T conditions	***4.2 GPa /1700 °C***	***1 GPa /1270 °C***	***3.4 GPa /1360 °C***	***4.5 GPa /1540 °C***
SiO_2	**40.96(34)**	*33.99(22)*	*32.70(26)*	*31.12(41)*
TiO_2	**2.60(13)**	*2.52(14)*	*2.47(10)*	*2.21(10)*
Al_2O_3	**10.08(12)**	*8.59(13)*	*8.50(13)*	*7.60(9)*
Fe_2O_3	**3.19(14)**	*2.14(7)*	*3.40(8)*	*3.80(16)*
MnO	**0.19(4)**	*0.24(4)*	*0.21(4)*	*0.22(3)*
MgO	**17.00(22)**	*17.48(24)*	*16.45(9)*	*17.29(24)*
CaO	**13.51(16)**	*23.35(12)*	*22.58(26)*	*21.12(20)*
Na_2O	**2.53(5)**	*0.75(3)*	*0.73(3)*	*0.88(5)*
K_2O	**1.75(3)**	*0.53(3)*	*0.54(3)*	*0.68(4)*
P_2O_5	**0.41(6)**	*0.97(7)*	*1.42(7)*	*1.39(4)*
Total	**92.24(32)**	*90.54(37)*	*89.00(33)*	*86.30(51)*

Table S2. EMPA results of olivine recovered from some runs.

	FOID2_RUN1	*FOID2_RUN2*
No. of points analyzed	*8*	*4*
Oxide	***1 GPa /1270 °C***	***3.4 GPa /1360 °C***
SiO_2	*41.98(36)*	*40.93(26)*
TiO_2	*0.08(5)*	*0.08(2)*
Al_2O_3	*0.10(3)*	*0.13(2)*
FeO	*2.36(46)*	*3.59(28)*
MnO	*0.18(3)*	*0.16(3)*
MgO	*54.49(52)*	*53.72(53)*
CaO	*1.03(14)*	*0.78(5)*
Na_2O	*0.03(3)*	*0.01(1)*
K_2O	*0.00(1)*	*0.01(1)*
P_2O_5	*0.11(4)*	*0.08(4)*
ClO^-	*n.a.*	*n.a.*
F^-	*n.a.*	*n.a.*
IrO_2	*n.a.*	*n.a.*
Total	*100.34*	*99.48*